Black phosphorus synthesized by solvothermal reaction from red phosphorus and its catalytic activity for water splitting

Akiyo Ozawa, Muneaki Yamamoto, Tetsuo Tanabe, Saburo Hosokawa, Tomoko Yoshida

Black phosphorus synthesized by solvothermal reaction from red phosphorus and its catalytic activity for water splitting

Akiyo Ozawa[1, 2*], Muneaki Yamamoto[3], Tetsuo Tanabe[3], Saburo Hosokawa[4, 5], Tomoko Yoshida[3]

1. Applied Chemistry and Bioengineering, Graduate School of Engineering, Osaka City University, 3-3-138, Sugimoto, Sumiyoshi-Ku, Osaka, Japan

2. Corporate Research Laboratories, Research & Development Division, Sakai Chemical Industry, Co., Ltd., 5-1, Ebisujima-Cho, Sakai-Ku, Sakai, Japan

3. Osaka City University Advanced Research Institute for Natural Science and Technology,

3-3-138, Sugimoto, Sumiyoshi-Ku, Osaka, Japan

4. Elements Strategy Initiative for Catalysts & Batteries (ESICB), Kyoto University, Kyotodaigaku Katsura, Nishikyo-ku, Kyoto 615-8245, Japan

5. Department of Molecular Engineering, Graduate School of Engineering, Kyoto University, Kyotodaigaku Katsura, Nishikyo-ku, Kyoto 615-8510, Japan

*Corresponding author: ozawa-a@sakai-chem.co.jp, +81-72-223-4117

Abstract

We have succeeded to synthesize black phosphorus (BP) with one-pot solvothermal reaction of red phosphorus (RP) in ethylenediamine (ED) used as a solvent. To examine the reaction mechanism, we have investigated the influence of the synthesis conditions on BP, and the valence of dissolved phosphorus in the solvent after the reaction. P^0 species and P^{3+} like species are very likely dissolved in ED as intermediates for BP production. Optimizing the reaction conditions, i.e., temperature, charging amount of RP in ED and particle size of RP, BP was synthesized with high yield. The synthesized BP have an extra peak at 10.2 º in X-ray diffraction pattern, which was assigned to stacking faults or periodic distortion in direction of the c axis by simulation of diffraction. The synthesized BP with Co-P cocatalyst showed high photocatalytic activity for hydrogen evolution from methanol aqueous solution under visible light irradiation.

1. Introduction

Photocatalytic water splitting has attracted attention as one of the solutions to moderate global warming.[1,2] Although various metal oxides have used as photocatalysts, most of them do not work with visible light owing to their quite wide band gap. Recently, black phosphorus (refers to as BP hereafter) has been studied as a candidate photocatalyst working under visible light.[3–6] It is a layered semiconductor having a narrow band gap which could be altered by changing its layer thickness.[7,8] The synthesis of BP is usually done at high temperature and pressure that makes the quantity synthesis difficult. Some new synthesizing methods of BP have been developed, for examples, a ball milling

method and chemical vapor depositions using red phosphorus (referred to as RP hereafter).[9,10] However, these methods seem difficult to apply for industrial scaled production. Recently, solution syntheses of BP suitable for mass production have attracted attention. Tian et al. have employed a solvothermal synthesis of BP nanosheets using white phosphorus and succeeded to synthesize BP showing high photocatalytic activity for water splitting.[11] Li et al. have produced composites of RP and BP for Li/K-ion storage from white phosphorus with the solvothermal synthesis using amine as a solvent. They have indicated that both primary amines with $–NH_2$ and secondary amines with –NH– could dissolve white phosphorus making precursor in BP synthesis.[12] Both studies, unfortunately, have used white phosphorus, which is toxic and flammable above 40 °C. On the other hand, RP is safely handled and widely used in industries. Therefore, the solution synthesis of BP using RP as starting material, if possible, would be very important for industrial synthesis. Dragulescu-Andrasi et al. have shown that potassium ethoxide can convert to soluble polyphosphide from RP.[13] Zhao et al. have produced agglomerates of very small BP nanosheet which have a wider band gap than RP by hydrothermal synthesis using ammonium fluoride aqueous solution and RP as reactants.[14] Liu et al. reported that synthesis of composite of BP/RP with high photocatalytic activity for water splitting from RP in amine solvent.[15] However, there are few reports on method to get high yield of BP and the synthesis mechanism of BP from RP were unclear.

In this study, we have applied one-pot solvothermal reaction with amines as a solvent and RP as a starting material to synthesize BP to be used as a photocatalyst of water splitting. By optimization of synthesis conditions in terms of concentrations and particle sizes of RP as a starting material, reaction temperature, and time, to get high yield of BP, we have succeeded in synthesis of BP. Synthesized BP was characterized by various methods, such as X-ray diffraction, scanning electron, and transmission electron microscopes. To understand mechanism of BP synthesis, i.e. dissolution of RP and precipitation of BP, P K-edge XANES spectra of filtrate, which was remained solvent after removing product by filtration, were measured. Formation mechanism and photocatalytic activity for hydrogen evolution were discussed.

2. Materials and Methods

2.1 Synthesis of BP

Samples were synthesized by one-pot solvothermal reaction changing reaction conditions; reaction temperature and time, and concentration of RP in ED and particle size of RP as indicated in Table 1. The following three types of RP were used, 23 μm (Wako pure chemical), 68 or 1300 μm (Koujundo chemical lab.) as starting materials. RP was dispersed in ED selected as a solvent. RP dispersed in the solvent is referred to as a slurry hereafter. The concentration of RP in the slurry (slurry concentration) was defined as, equation (1)

$$\text{Slurry concentration} = \text{RP (g)} / \text{ED (L)}, \quad (1)$$

where RP and ED are based on mass (g) and volume (L), respectively.

The slurry was put into a Teflon-lining autoclave and heated at various temperatures for 12-48 hours. After natural cooling, the slurry was filtered and rinsed with ethanol followed by distilled water. The synthesized samples were dried for 12 hours in vacuum.

Commercial available BP, purchased from Smart element, was used as a reference after crushing (referred to as BP (ref)).

2.2 Cocatalyst loading on BP

For photocatalytic water splitting, Pt or Co was loaded on BP as a cocatalyst as follows. Pt cocatalyst was loaded on sample 11 by a photodeposition method using 30 vol% methanol aqueous solution

containing H_2PtCl_6 as Pt source.[16] The loading amount of Pt was adjusted to be 0.5 mol% as Pt metal. The Pt loaded BP is referred to as Pt/sample 11.

Co/sample 11 was prepared by the one-pot reaction in the same way as sample 11 adding cobalt acetylacetonate into the solvent. Three samples were prepared changing the amount of cobalt acetylacetonate in the solvent. The loaded amount of Co in the prepared samples were determined by Energy Dispersive X-ray spectroscopy (EDS) of Scanning Electron Microscope (SEM) and found to be 1.1, 2.0, 2.3 mol% as Co metal in the samples.

2.2 Characterization of the samples

The crystal structure of the samples was identified by X-ray diffraction analysis (XRD) (RIGAKU, MiniFlex). Crystal size of the sample was calculated using the Scherrer equation from 020 peak of BP in XRD patterns. Diffuse reflectance spectra of the samples were obtained by using a UV-vis-NIR spectrometer (UV-vis) (JASCO, V-670) in the wavelength range of 200–1200 nm. The reflectance was converted to absorbance by the Kubelka–Munk function referring that of $BaSO_4$ as a standard. The band gaps (Eg) of the samples are determined by the equation $(\alpha h\nu)^{1/n} = A(h\nu - Eg)$, where α, n, A, and Eg are the absorption coefficient, light frequency, proportionality constant, and band gap, respectively.[17] In this study, n=1/2 was used.

Morphology and particle sizes of the samples were observed by a transmission electron microscope (TEM) (JEOL, JEM-ARM 200F Cold) and Scanning Electron Microscope (SEM) (JEOL, JSM-7000F). Low resolution TEM and Energy Dispersive X-ray spectroscopy (EDS) analysis were conducted by JEM-2100F (JEOL). Impurities in the samples were determined by X-ray fluorescence spectroscopy (RIGAKU ZSX Primus II). P K-edge XANES spectra of the filtrate after the solvothermal reaction were measured with the BL6N1 at Aichi Synchrotron at room temperature in the fluorescence mode. Raman spectra were obtained using laser Raman spectrophotometer (Jasco, NRS-3100). Excitation light with a 532 nm wavelength was focused on the sample in air. The particle size of RP was determined from median diameter analyzed by Laser diffraction/scattering particle size distribution analyzer after ultrasonic dispersion in ion exchange water (MicrotracBEL, MT3000II).

The specific surface areas of the samples were determined by the Brunauer–Emmet–Teller (BET) method (MOUNTECH, Macsorb HM-1220). Chemical states of the samples were investigated by X-ray photoelectron spectroscopy (XPS) (Shimadzu, ESCA-3400HSE). Binding energy was calibrated using the C 1s peak at 284.6 eV.

2.3 Evaluation of photocatalytic activity for hydrogen evolution

To evaluate the half-reaction of water splitting, photocatalytic activities of the samples were examined by hydrogen evolution from methanol aqueous solution at room temperature under visible light irradiation. Methanol was used as a scavenger. The reaction is referred simply to as hydrogen evolution hereafter. The sample of 0.05 g was put into 10 mL of 20 vol % methanol aqueous solution in a quartz cell under He gas flow with a flow rate of 5 mL/min. The cell was irradiated with visible light ($\lambda > 420$ nm) given by a 300 W xenon lamp with cutting UV light by a cut-off filter, L-42 (Opto Sigma, SCF-50S-42L). The hydrogen evolution rate was analyzed with a gas chromatograph every hour for 5 hours (Shimadzu, TCD-GC, GC-8A).

3. Results

3.1 Formation of BP

To synthesize BP in solvothermal reaction, we carried out reaction at various conditions as shown in Table 1. Note that some samples are duplicated for easy comparison. The relative BP yield was determined by a ratio of the intensity of 020 peak of BP around 17 º to the sum of the intensity of RP at 15 º and BP of 020 peak. BP was formed above 150 °C, and the yield was highest at 160 °C as shown in comparison of sample 1, 2, 3, and 4. Above 170 °C, the BP yield decreased, some unidentified reactions occurred, resulting in transparent solids together with BP and RP. Therefore, we selected 160 °C as the best reaction temperature, and carried out subsequent syntheses at 160 °C.

To improve the BP yield, the effects of reaction time, particle size of RP, and RP concentration in the slurry on the yield of BP were evaluated. Effects of reaction time, particle size of RP and RP concentration in the slurry are also seen in comparison of samples 3, 5, and 6 and that of samples 5, 7 and 8, and that of samples, 9, 10, 7 and 11, respectively in Table 1. It should be noted that longer reaction times did not give a higher yield of synthesized BP. The smaller particle size did not give the higher yield too. The surface of RP was usually oxidized by water and oxygen in the air, phosphate group would be formed preferentially on the surface of RP.[9] Therefore, smaller RP particles have more phosphate groups, resulting in the prohibition dissolution of P into ED. On the other hand, the dissolution rate of the larger particles might be very low and suppress the formation of BP in sample 8 of which surface was black and the inside was red, indicating that BP covers its surface, while its inside remained RP. Therefore, medium-sized particles would be better. Additionally, a higher slurry concentration gave the higher yield, and the yield was saturated above 15 g/L as shown in Table 1. Crystal sizes of the samples in Table 1 became larger with increasing the yield. In element analysis determined by XRF measurement, sample 7 has mostly consisted of P, impurities were 4.5% O and very low another element, which was nearly the same as that of RP used as a starting material (see Fig. S1).

As the BP yield appreciably changed with the slurry concentration, detailed characterization of samples were made as shown in Fig. 1, 2, and 3 for SEM images, XRD patterns, and UV-vis , respectively with comparisons of the samples of 7, 9, 10, and 11. As seen in the SEM images in Fig. 1, all samples exhibited completely different morphology from that of RP used as the starting material. Probably nanometer-sized layered BP aggregated to make particles, which were smaller than original particles of RP used as the starting material.

The particle size of the products became larger with increasing the slurry concentration (Fig. 1). Also, the product was mostly BP at the slurry concentration of sample 7 or 11 as seen XRD (Fig. 2) and UV-Vis (Fig.3). In UV-vis diffused reflectance spectra of the below 7.5 g/L (sample 9 or 10), the spectrum was assigned sum of absorption of RP and BP. This agrees with the indication of XRD. The peak at 450 nm could be assigned small RP particles shifted shorter wavelength by quantum effect, and that over 650 nm was due to nanosized BP (Fig. 3).[18] When the slurry concentration was at 15 g/L (sample 7), absorption due to BP became prominent. Since samples 7 and 11 shows a quite similar character in their morphology and optical properties, the yield of BP was saturated at 15 g/L. For the photocatalytic reduction test, we have prepared BP with same condition for sample 11.

To understand the formation process in detailed, P K-edge XANES spectrum of the filtrate after the solvothermal reaction of sample 3 was measured together with a commercial BP, RP, and P_2O_5 as reference (Fig. 4). A peak appeared at 2145 eV is assigned to P^0 species and peaks at 2147-2155 eV are probably due to P^{3+} species. These results indicate that RP was dissolved in the solvent as at least

two phosphorus species. Either or both species should be involved in the formation of BP, which is discussed later.

3.2 Micro or crystalline structure of synthesized BP

Crystalline structure of produced BP particles was derived from the XRD pattern and HRTEM images. In XRD pattern, the intensity of 020 peak around 17 ° increased with the decrease of RP peak at 2θ = 15.2 ° (Fig. 2), which indicates RP content in the sample decrease with the formation of BP. In XRD, all peaks except one at 10.2 ° and 30.1 ° appeared at the same angles of the reference XRD peaks of BP (PDF 076-1967). In the reference XRD, the peak at 2θ = 10.2 ° and 30.1 °, which corresponds to the lattice spacing of 8.6 Å and 2.8 Å respectively, are not appearing. These diffraction peaks did not derive from impurities, considering sample 7 consisted almost P and 4.5% O by XRF measurement in Fig. S1. According to a theoretical calculation by Asahina and Morita the lattice parameters of fully crystalized BP are a = 3.314 Å, b = 10.478 Å, and c = 4.376 Å.[19] The observed lattice spacing of 8.6 Å is about two times of the lattice parameter c, indicating stacking fault or periodic distortion in direction of the c axis as sometimes appearing in crystal structure. The most probable cause is substitution of two P atoms in the unit cell by either vacancies or some other elements like O, or H as shown in Fig. 5 (b) with comparison of normal unit cell of BP in Fig 5 (a). The powder diffraction pattern consisting the lattice model was simulated using VESTA,[20] a three-dimensional visualization system for crystallographic studies and electronic state calculations. The simulation showed a strong peak at 2θ = 10.1° without significant changes in other diffraction peaks positions (Fig. 5 (c, d)). Such periodic distortion or introduction of stacking fault would retard the growth of crystalline in the layered direction as appeared in the SEM images. At the same time, this suggests the mechanism of BP deposition form the solvent. The formation of BP is also confirmed by HRTEM image and Raman spectra as shown in Fig. 6 and 7. The lattice fringe of 0.504 nm appeared in Fig. 6 corresponds to the lattice spacing of (020), which is the indication of the layered structure of BP.

Low resolution TEM images and EDS maps from TEM of the samples are shown in Fig. S2. The TEM images clearly show that the samples were formed by stacking small elongated particles. The EDS maps and spectrum indicate that sample 7 was consisted mostly of P with a few impurity oxygen (O), which agrees with sample composition determined by X-ray fluorescence analysis given in Fig. S1. Specific surface area of sample 7 was 1.4 m^2/g, which is well corresponding to the image of the aggregated particles shown in SEM (Fig. 1) and TEM (Fig S2). Wide range XPS spectrum and detailed P 2p XPS spectrum of sample 7 are shown in Fig. S3 together with that of BP (ref). P 2p XPS spectrum was divided into 6 peaks. Two peaks at 128.9 and 129.8 eV were attributed to elemental state of P. Other four peaks, at 130.5, 131.3, 132.5 and 133.6 eV were shifted with 1.6, 2.4, 3.6, and 4.7 eV respectively from the peak at 128.9 eV, and were assigned to P-O-P bonding, O=P-O species, -P-N bonding [31], and P_2O_5 respectively[15 21]. These observations indicate that the surface of the samples was slightly oxidized and a small amount of ED was remained as adsorbate.

Figure 7 shows Raman spectra of sample 7 together with those of RP and BP (ref). Sample 7 clearly shows characteristic peaks of BP assigned as A_g^1 at 365 cm^{-1}, B_{2g} at 442 cm^{-1}, and A_g^2 470 cm^{-1}.[22] The peak at 388 cm^{-1} is assigned to the characteristic peak of P–O bond.[23] From these observations, we have concluded that a new method to synthesize BP with one-pot solvothermal reaction of RP is

established. Further, the synthesized BP under the optimized condition exhibited the layered structure, one of the most important characteristics of BP. However, it included some periodic distortion or stacking fault, which likely inhibited BP to be larger sheet.

3.3 Photocatalytic activity tests

In the photocatalytic hydrogen evolution tests, a sample synthesized under the same condition with sample 11 was used because of its highest yield of BP. Either Co or Pt was loaded as a cocatalyst. As for Co, 1.1 % of Co loaded sample (Co/sample 11) was used for the test. The tests were also done for sample 11 without the cocatalyst and RP with the Pt cocatalyst. Figure 8 shows the integrated amount of evolved hydrogen under visible light irradiation with the reaction time. The sample without the cocatalyst hardly showed the hydrogen evolution. Co cocatalyst significantly enhanced the hydrogen evolution, while Pt was a little. The cause of the improvement is discussed later. The results for 24 hours of the activity tests of the Co/sample 11 are shown in Fig. S4. Although hydrogen evolution rate gradually decreased with the test time, it continued even after 24 hours. The sample before and after the test was characterized by TEM, EDS, and XPS analysis. The morphology of the sample before the test was an aggregation of elongated layered particles, similar to the sample without Co loading as shown in Fig. S2. However, the sample after the test exhibited coexistence of elongated layered particles and round small particles (Fig. S5). The EDS analysis of the sample before the test showed that loaded Co was well dispersed over the sample surface, while the distribution of Co in the sample after the test was not uniform; Co was not included in some particles (Fig. S7).

Discussion

1) Mass balance in synthesis and dissolution of RP in ED

Mass balance among charged RP, residue (sample), P dissolved in filtrate (ED), and produced BP was determined after the separation of the residue and the filtrate room temperature (RT) as follows for samples of 9, 10, 7, and 11 synthesized under the same condition except initial charged amount of RP. After the synthesis, firstly, remained solvent and produced solid were separated by filtration. Then the amounts of remained RP and produced BP in the residue were determined from the respective fraction determined by X-ray analysis given in Table 1. The results are given in Table 2, the table shows BP yield is quite high in sample 11. It is also quite important to note that P was dissolved in ED showing a saturation concentration around 6.0 g/L suggesting the solubility limit at RT. Since the solubility should be higher at higher temperatures, significant amount of P could be dissolved in ED at 160 ºC. The precipitation of BP would proceed when the concentration of P in ED became the solubility limit at the reaction temperature and also during cooling owing to the reduction of the solubility. On the other hand, when the P concentration did not attain the solubility limit like sample 9 in which the charged amount of P was too small, and also sample 8 in which the particle size of charged RP is too large to be fully dissolved, the precipitation of BP would be suppressed. All these observations confirm that the BP synthesis proceeds as, firstly RP is dissolved in ED as P^0 and/or P^{3+} states and then BP precipitates when the concentration of P in ED becomes the saturation level.

2) Mechanism of BP formation

Here discussed is the precipitation mechanism of BP from P dissolved in ED. It is known that ED dissolves some metal ions making a chelate consisting of a five-membered ring with a metal ion in its center.[24,25] In the present case, ED could be chelated with P on the surface of RP like in Fig. 9 (a), or one NH_2 is bonded to P as shown in Fig. 9 (b) and dissolved as P^{3+} species as supported in XANES spectra. Considering the existence of P^0 species, the P^{3+} species would be equilibrated with the P^0 species. Li et al. reported the existence of soluble polyphosphorus (P_{16}^{2-}) in ED.[12] In this study, the P^0 species is probably making polyphosphorus like P_{16}^{2-}. Considering these points, the nucleation of BP may proceed through aggregation of the soluble polyphosphorus like scheme (1). It is considered that the periodic distortion or stacking faults structure seen in XRD pattern is accompanied during the aggregation of the polyphosphorus to relax the lattice distortion.

$$\text{RP} + \text{ED (en)} \rightleftharpoons [P^{3+}(\text{en})_x] \rightleftharpoons P^0\,(\text{Polyphosphorus}) \rightleftharpoons \text{BP} \qquad (1)$$

To confirm the above the hypothesis, further study is needed.

2) Photocatalytic activity for hydrogen evolution

As seen in Fig. 8 the photocatalytic activity of BP was confirmed when cocatalysts were used. However, the effect of Pt cocatalyst is less compared to significant improvement by Co cocatalyst. Here, we discuss the cause of the improvement based on characterization for chemical states of Pt and Co observed by XPS and EXAFS. Figure 10 (a) and (b) show Pt 4f XPS spectrum of Pt/sample 11 and Co 2p XPS spectrum of the Co/sample 11. The XPS spectrum of Pt/sample 11 shows two main peaks at 71.9 and 75.1 eV, attributed to a metallic state of Pt^0 $4f_{7/2}$ and Pt^0 $4f_{5/2}$, respectively (Fig. 10 (a)).[26] In contrast, the chemical state of Co on sample 11 was attributed to Co bonded to P.[27] This indicates the cause of the significant improvement is likely the existence of Co phosphide. To determine what kind of Co phosphide was made on BP, Co K-edge EXAFS was observed for sample 11 loaded different amounts of Co (Fig. S9 (a) and (b)). Since both Co K-edge XANES spectrum and EXAFS oscillation of 2.3% Co were similar to those of Co_2P, the chemical state of 2.3 % Co loaded on sample 11 was assigned to Co_2P. For lower Co loaded samples, Co K-edge XANES and EXAFS oscillation on 1.1 or 2.0% were different from those of Co_2P but similar to those of Co-P bonding as seen Fig S10. The Co 2p peak due to Co-P was shifted lower binding energy with decreasing the loading amount of Co, which indicates the decrease of the number P atoms coordinated to a Co atom.[28] Considering XPS and EXAFS of Co, the chemical state of 1.1% Co loaded on sample 11 would be amorphous like Co_xP, in which a Co atom is surrounded by fewer numbers of P atoms than that in crystalized Co_2P.

Popczun et al. have reported that the cobalt phosphide is highly active electrocatalysis for hydrogen evolution because it significantly decreases the reduction potential of water.[29] Cao et al. have demonstrated that CoP/CdS showed higher photocatalytic hydrogen evolution than Pt/CdS.[30] In the case of BP, Tian et al. have reported that amorphous CoP as a cocatalyst enhances hydrogen evolution than Pt cocatalyst, which corresponds to the present result.[23] These observations supports that Co on

BP in the chemical form of Co_xP works as the cocatalyst of BP on the photocatalytic hydrogen evolution.

As shown in Fig. 4S, the catalytic activity gradually decreased in long time use. One of the reasons for the gradual reduction is the aggregation of loaded Co in the sample shown in Fig. S6 and S7. The aggregation of the loaded Co is likely the cause of the reduction of the hydrogen evolution as seen in Fig. S4. Other reasons are morphology change as seen in Fig. S5, which accompanies the widening and lower energy shift of the main peak of P 2p in XPS spectra (Fig. S8). Since BP has high carrier mobility in the parallel direction to the BP sheet, the morphology change appeared in Fig. S5 would reduce the mobility of photoexcited holes and electrons resulting in the reduction of the photocatalytic activity. For air-exposed BP, Edmonnds et al. observed a similar change in P 2p XPS spectra[21], while Island et al. observed reduction of conductance of BP[31]. Considering these observations, the conductivity of the Co/sample 11 after the test was very likely decreased by degradation with superoxide generated under photo irradiation[32]. The change of morphology and the reduction of conductance were also likely to the cause of the reduction of hydrogen evolution.

Conclusions

We have succeeded in synthesizing black phosphorus (BP) employing one-pot solvothermal reaction of red phosphorous (RP) and ethylenediamine (ED) used as a solvent. The method is safer and can synthesize larger amounts of BP than conventional methods using white phosphorous or high pressure and temperature. Optimizing reaction condition (reaction temperature and time, slurry concentration and particle size of RP), BP was synthesized with quite high yield.

The synthesized BP exhibits sheet-like morphology with a fully crystalized layered structure excepted periodic distortion or stacking faults in the direction of c-axis. However, the sheet-width or crystalline size of the synthesized BP was not large.

The BP synthesis very likely proceeds through the dissolution of RP in ED to be P^0 and/or P^{3+} states and BP precipitation from dissolved P. The periodic distortion or stacking faults were very likely introduced in the synthesis process to relax accumulated distortion and inhibit the growth of the sheet width.

The synthesized BP showed high photocatalytic activity with an aid of Co-P cocatalyst for hydrogen evolution from methanol aqueous solution under visible light irradiation. However, the activity decreased after long time use owing to the aggregation of Co-P cocatalyst and morphology change of BP.

To increase the photocatalytic activity and durability, larger sheets are preferable, because they should have less stacking faults and terminated bonds at the sheet edge. Therefore enlargement of the sheet width of the synthesized BP is necessary.

Conflicts of interest

There are no conflicts to declare.

Acknowledgments

This study was supported by JSPS KAKENHI Grant Number JP16H06440 (Synthesis of Mixed Anion Compounds toward Novel Functionalities). We thank Mr. Yuta Yamamoto in High Voltage Electron Microscope Laboratory, Nagoya University for assistance with the HRTEM measurements.

References

1 A. Kudo and Y. Miseki, *Chem. Soc. Rev.*, 2009, **38**, 253–278.
2 K. Takanabe, *ACS Catal.*, 2017, **7**, 8006–8022.
3 T. Sakthivel, X. Huang, Y. Wu and S. Rtimi, *Chem. Eng. J.*, 2020, **379**, 122297.
4 Z. Shen, S. Sun, W. Wanjun, L. Jianwen, L. Zhifeng and Y. C. Jimmy, *J. Mater. Chem.*, 2015, **3**, 3285–3288.
5 T. Lee, S. Kim and H. Jang, *Nanomaterials*, 2016, **6**, 194.
6 H. Uk Lee, S. C. Lee, J. Won, B. C. Son, S. Choi, Y. Kim, S. Y. Park, H. S. Kim, Y. C. Lee and J. Lee, *Sci. Rep.*, 2015, **5**, 1–6.
7 A. Castellanos-Gomez, L. Vicarelli, E. Prada, J. O. Island, K. L. Narasimha-Acharya, S. I. Blanter, D. J. Groenendijk, M. Buscema, G. A. Steele, J. V. Alvarez, H. W. Zandbergen, J. J. Palacios and H. S. J. Van Der Zant, *2D Mater.*, 2014, **1**, 025001.
8 V. Eswaraiah, Q. Zeng, Y. Long and Z. Liu, *Small*, 2016, 3480–3502.
9 M. Nagao, A. Hayashi and M. Tatsumisago, *J. Power Sources*, 2011, **196**, 6902–6905.
10 X. Li, B. Deng, X. Wang, S. Chen, M. Vaisman, S. I. Karato, G. Pan, M. L. Lee, J. Cha, H. Wang and F. Xia, *2D Mater.*, 2015, **2**, 31002.
11 B. Tian, B. Tian, B. Smith, M. C. Scott, Q. Lei, R. Hua, Y. Tian and Y. Liu, *Proc. Natl. Acad. Sci.*, 2018, **115**, 4345–4350.
12 Y. Li, S. Jiang, Y. Qian, Y. Han, J. Zhou, T. Li and L. Xi, *Chem. Commun.*, 2019, **55**, 6751–6754.
13 A. Dragulescu-Andrasi, L. Z. Miller, B. Chen, D. T. McQuade and M. Shatruk, *Angew. Chemie - Int. Ed.*, 2016, **55**, 3904–3908.
14 G. Zhao, T. Wang, Y. Shao, Y. Wu, B. Huang and X. Hao, *Small*, 2017, **13**, 1602243.
15 F. Liu, R. Shi, Z. Wang, Y. Weng, C. Che and Y. Chen, *Angew. Chemie*, 2019, **131**, 11917–11921.
16 J. M. Herrmann, J. Disdier and P. Pichat, *J. Phys. Chem.*, 1986, **90**, 6028–6034.
17 Q. Gu, K. Zhu, N. Zhang, Q. Sun, P. Liu, J. Liu, J. Wang and Z. Li, *J. Phys. Chem. C*, 2015, **119**, 25956–25964.
18 Y. Xu, Z. Wang, Z. Guo, H. Huang, Q. Xiao, H. Zhang and X. F. Yu, *Adv. Opt. Mater.*, 2016, **4**, 1223–1229.
19 H. Asahina and A. Morita, *J. Phys. C Solid State Physics,* 1984, **17**, 1839–1852.
20 K. Momma and F. Izumi, *J. Appl. Crystallogr.*, 2011, **44**, 1272–1276.
21 M. T. Edmonds, A. Tadich, A. Carvalho, A. Ziletti, K. M. O'Donnell, S. P. Koenig, D. F. Coker, B. Özyilmaz, A. H. C. Neto and M. S. Fuhrer, *ACS Appl. Mater. Interfaces*, 2015, **7**, 14557–14562.
22 R. Fei and L. Yang, *Appl. Phys. Lett.*, 2014, **105**, 083120.
23 B. Tian, B. Tian, B. Smith, M. C. Scott, R. Hua, Q. Lei and Y. Tian, *Nat. Commun.*, 2018, **9**, 1397.

24 Y. Xie, H. L. Su, X. F. Qian, X. M. Liu and Y. T. Qian, *J. Solid State Chem.*, 2000, **149**, 88–91.
25 Y. Xie, H. Su, B. Li and Y. Qian, *Mater. Res. Bull.*, 2000, **35**, 675–680.
26 Y. Z. Yang, C. H. Chang and H. Idriss, *Appl. Catal. B Environ.*, 2006, **67**, 217–222.
27 Y. Zhong, L. Yin, P. He, W. Liu, Z. Wu and H. Wang, *J. Am. Chem. Soc.*, 2018, **140**, 1455–1459.
28 Z. Jin, P. Li and D. Xiao, *Green Chem.*, 2016, **18**, 1459–1464.
29 E. J. Popczun, C. G. Read, C. W. Roske, N. S. Lewis and R. E. Schaak, *Angew. Chemie*, 2014, 5427–5430.
30 S. Cao, Y. Chen, C. Wang, X. Lv and W. Fu, *Chem. Commun.*, 2015, **51**, 8708–8711.
31 J. O. Island, G. A. Steele, H. S. J. Van Der Zant and A. Castellanos-gomez, *2D Mater.*, **2**, 11002.
32 Q. Zhou, Q. Chen, Y. Tong and J. Wang, *Angew. Chemie - Int. Ed.*, 2016, **55**, 11437–11441.

Table 1. Synthesis conditions and the result of various characterization of samples.

Sample No.	Reaction temp. (°C)	Reaction time (h)	RP particle size (μm)	Slurry conc. of RP (g/L)	Band Gap	RP X-ray peak intensity[a]	BP X-ray peak intensity[b]	BP /(RP+BP) %[c]	Crystal size of BP[d]
1	140	12	23	15	1.88	397	14	3.3	-
2	150	12	23	15	1.56	288	35	10.7	-
3	160	12	23	15	1.55	183	108	37.2	68 (17)
4	170	12	23	15	1.55	165	63	27.7	-
3	160	12	23	15	1.55	190	108	36.3	68 (17)
5	160	24	23	15	1.55	190	280	59.6	298 (16)
6	160	48	23	15	1.55	211	176	45.4	109 (10)
5	160	24	23	15	1.55	142	280	66.3	298 (16)
7	160	24	68	15	1.55	29	542	94.9	195 (10)
8	160	24	1300	15	1.88	247	3	1.2	-
9	160	24	68	3.75	1.6	222	9	3.8	-
10	160	24	68	7.5	1.6	176	101	36.5	178 (7)
7	160	24	68	15	1.55	29	542	94.9	195 (8)
11	160	24	68	30	1.56	18	551	96.8	219 (7)

X-ray peak intensities of RP [a] and BP [b] were taken from X-ray diffraction peak appeared around 15.4 º and 17 º respectively. The relative yield of BP [c] was calculated as the fraction of b to a + b. Crystal sizes [d] were calculated from the 020 peak of BP. For some samples, their crystal size are not given owing to large uncertainty in determination. Note samples 3 and 7 are duplicated for easy comparison.

Table 2. Mass balance among charged RP, residue after filtration (sample), P dissolved in filtrate (ED), produced BP in residue, and BP yield for samples 9, 10, 7, and 11 given in Table 1.

Sample No.	RP initially charged (mg) (Slurry concentration (g/L))	Residue (sample) (mg)	P dissolved in filtrate (ED) (mg) (Concentration (g/L))	Produced BP in residue (mg)	BP yield (%)
9	75 (3.75)	15	60 (3.0)	0.6	0.8
10	150 (7.5)	36.9	113.1 (5.7)	13.5	9.0
7	300 (15)	190.7	109.3 (5.5)	181.0	60.3
11	600 (30)	479	121 (6.1)	463.9	77.3

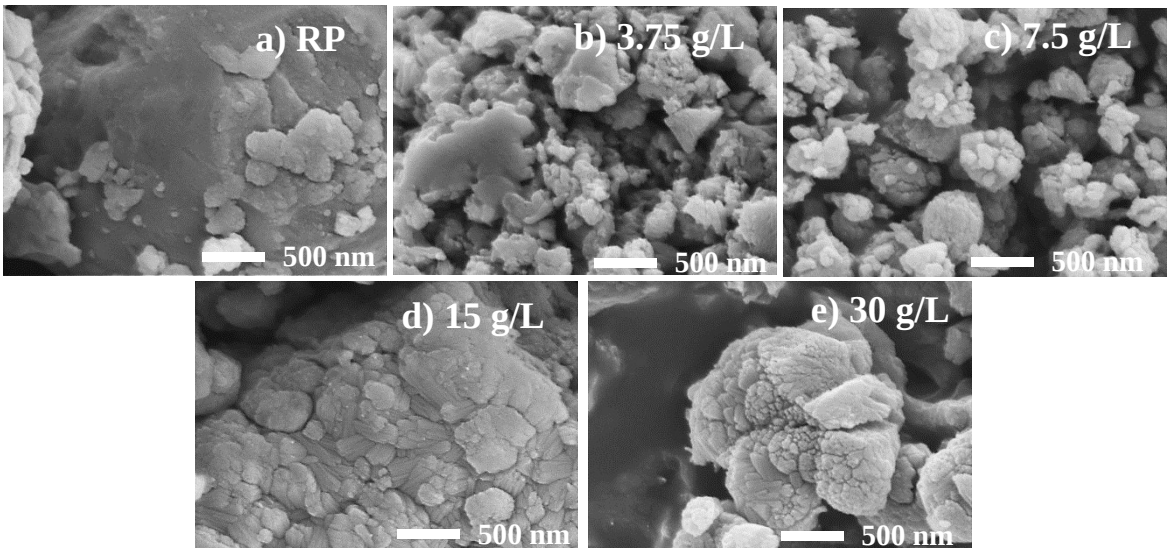

Fig. 1. SEM images of RP and the synthesized samples under different slurry concentrations. a) RP with 68 μm, b) sample 9, c) sample 10, d) sample 7, and e) sample 11. The scale bars in each figure are 500 nm.

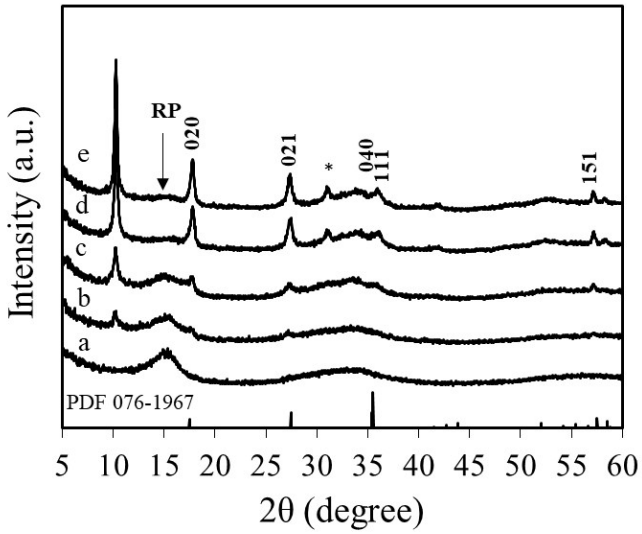

Fig. 2. XRD pattern of the samples respective to the SEM images in Fig. 1. Reference pattern of PDF076-1976 in JCPDF card is given for comparison. Peak marked with asterisk are unidentified.

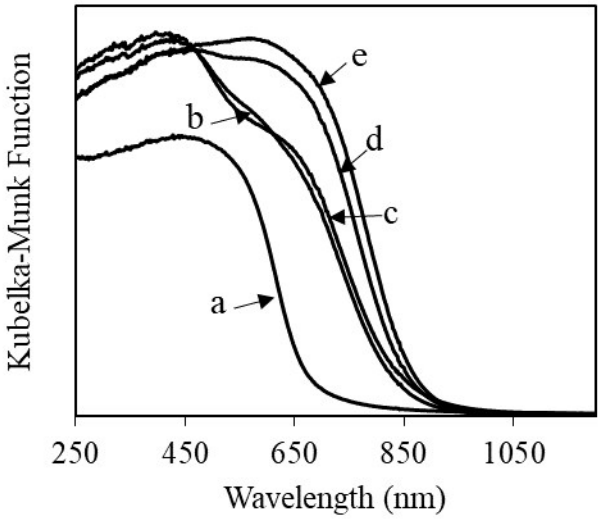

Fig. 3. UV-vis diffused reflectance spectra of the samples respective to the SEM images in Fig. 1.

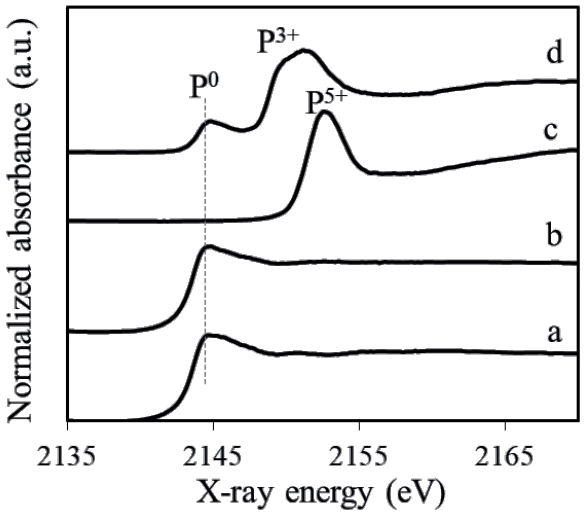

Fig. 4. P K-edge XANES of a) BP (ref), b) commercial RP (Wako), c) P_2O_5 (Wako), and d) filtrate in the reaction of sample 3.

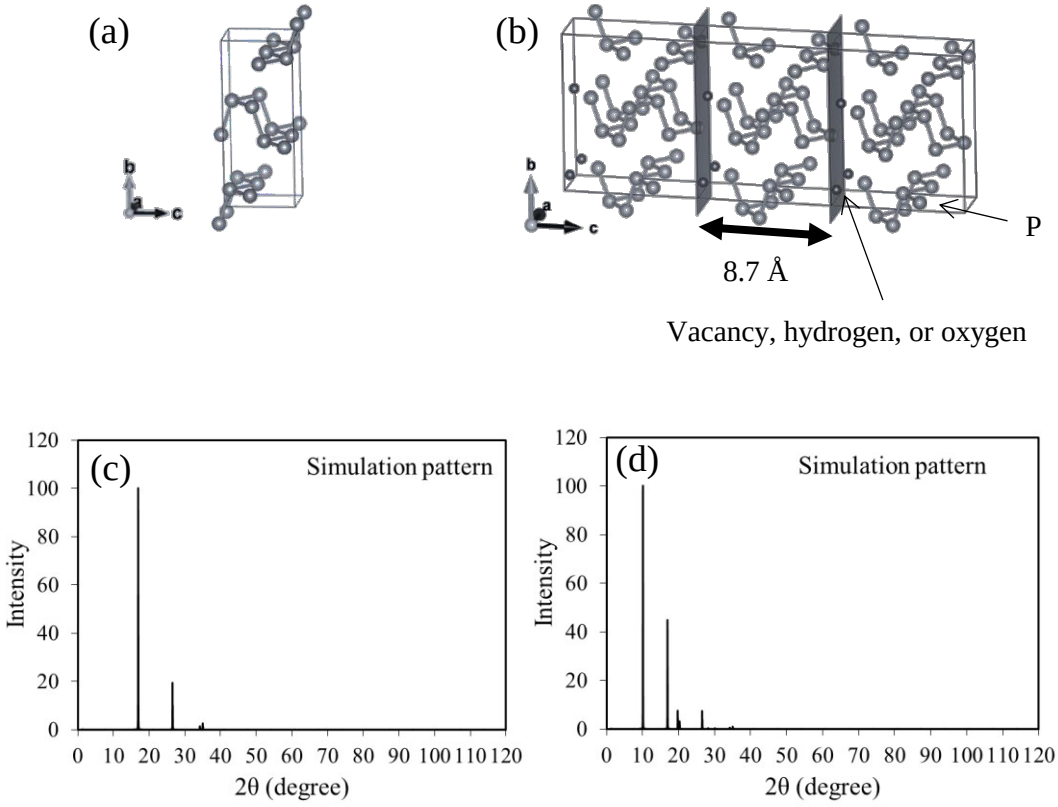

Fig. 5. (a) Unit cell of crystalline BP, (b) proposed crystal structure image of the sample 7. (c) and (d) are simulations of X-ray diffraction patterns corresponding respectively to (a) and (b) performed by VESTA program. (d) was simulated with vacancy. In the simulation, periodic stacking faults in (b) is assumed to be caused by vacancies.

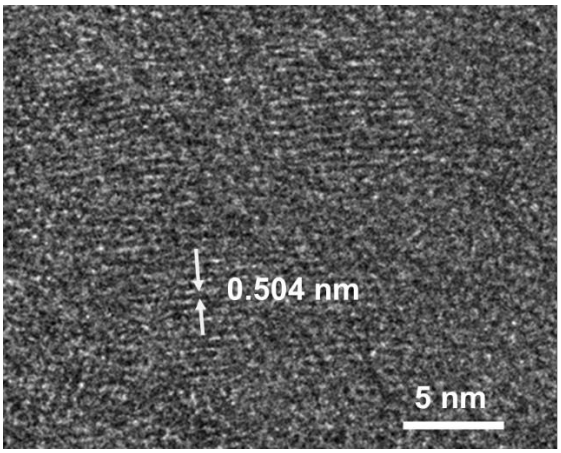

Fig. 6. HRTEM image of sample 7.

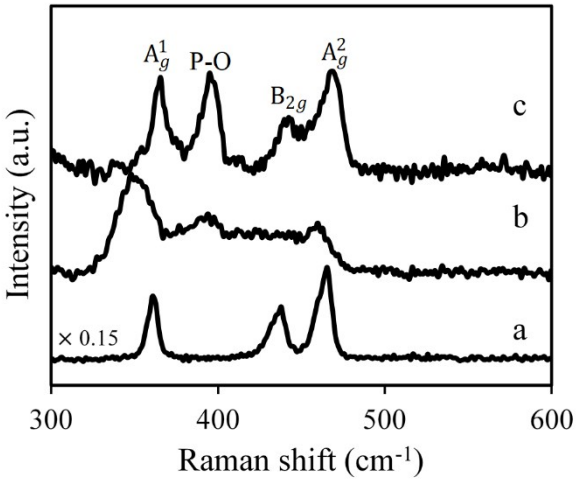

Fig. 7. Comparison of Raman spectra of a) BP (ref), b) commercial available RP, and c) sample 7.

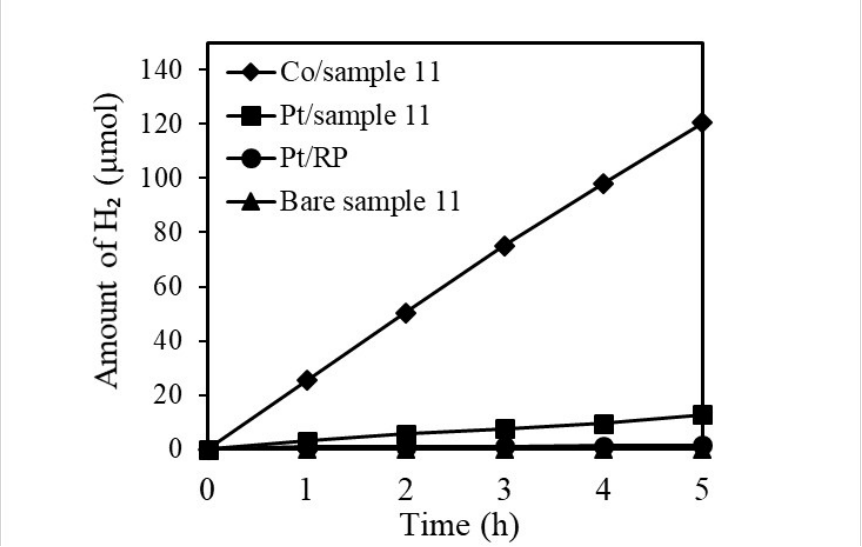

Fig. 8. Hydrogen evolution in water splitting with methanol aqueous solution under visible light irradiation for, a) bare sample 11(triangle), b) Pt/RP (circle), c) Pt/sample 11(square), and d) Co/sample 11(diamond).

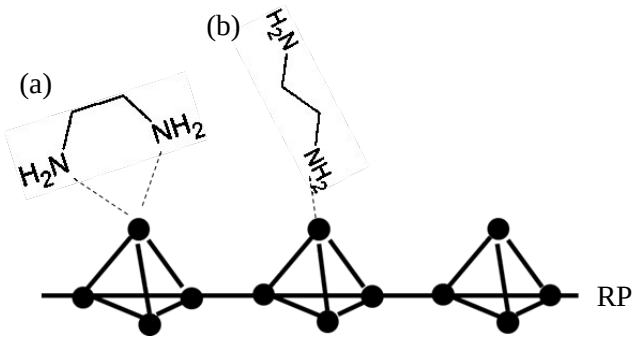

Fig. 9. Proposed mechanism of RP dissolution in ED.

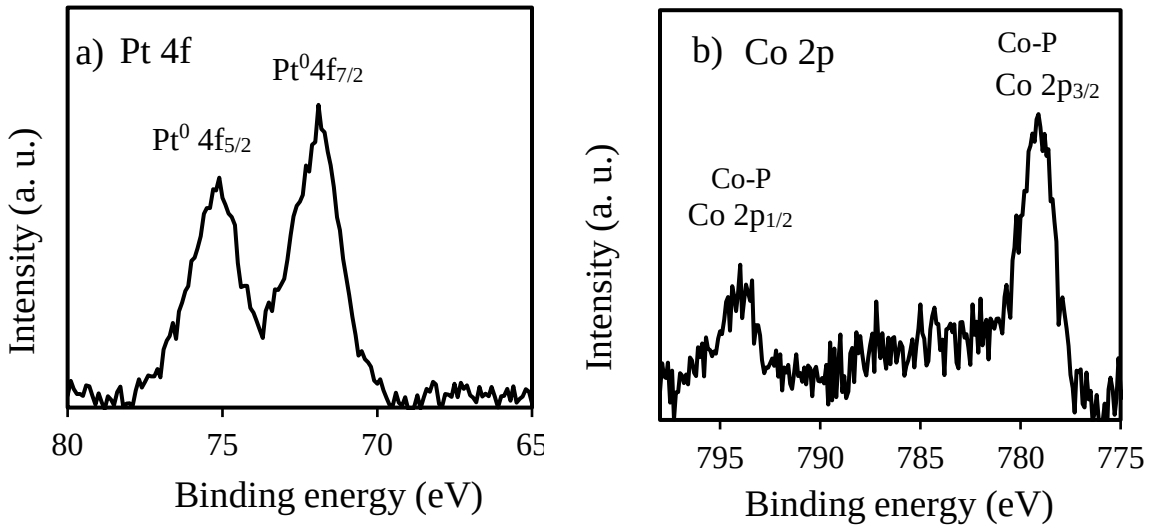

Fig. 10. a) Pt 4f XPS spectrum of Pt/sample 11, b) Co 2p XPS spectrum of Co/sample 11.

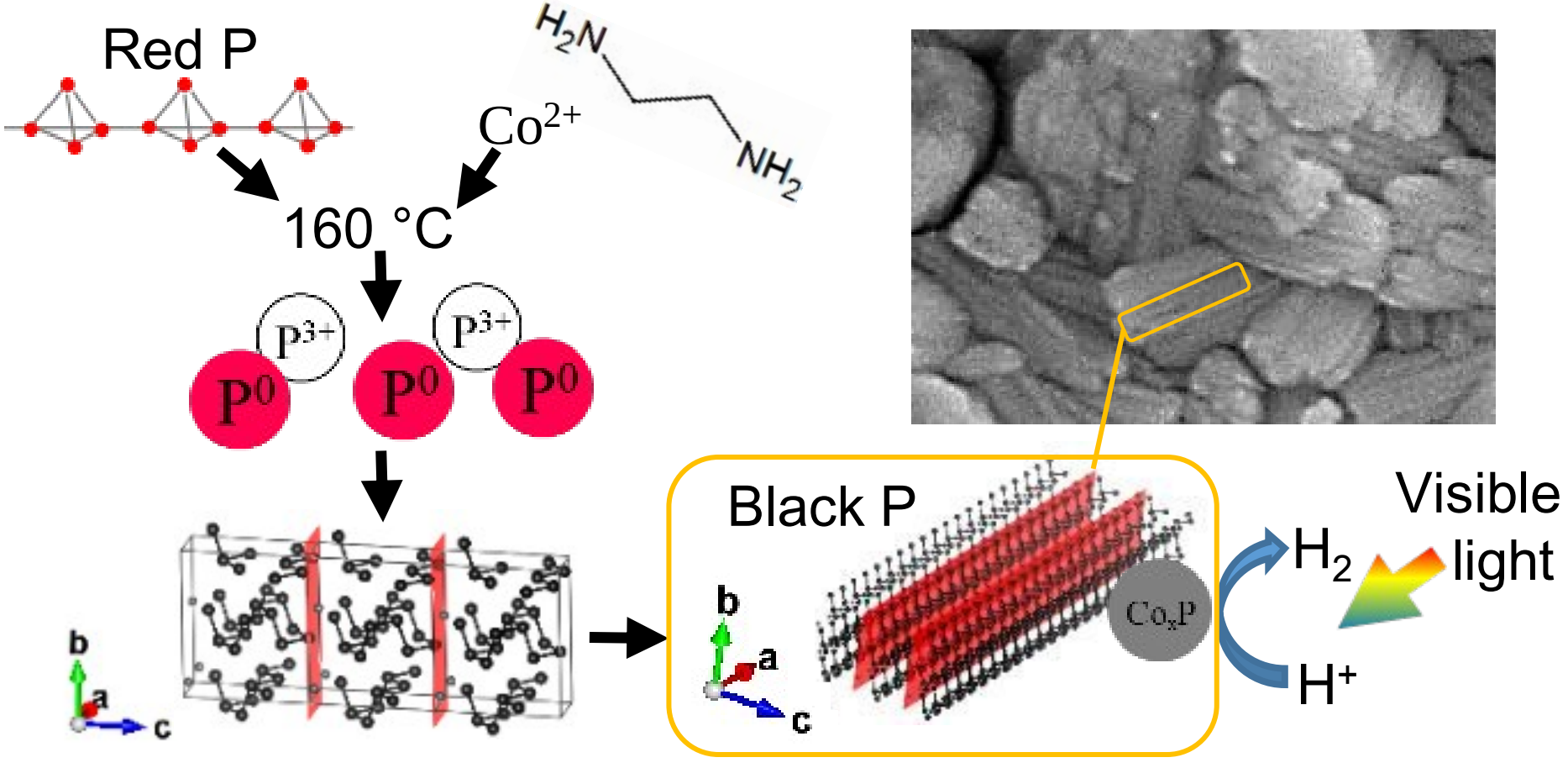
Red P
H_2N
NH_2
Co^{2+}
160 °C
P^{3+}
P^{3+}
P^0
P^0
P^0
b
a
c
Black P
b
a
c
Co_xP
H_2
H^+
Visible
light